ACS APPLIED MATERIALS & INTERFACES

Research Article

www.acsami.org

Catalyst-Free, Selective Growth of ZnO Nanowires on SiO_2 by Chemical Vapor Deposition for Transfer-Free Fabrication of UV Photodetectors

Liping Xu,[†,‡,§] Xin Li,[‡,§] Zhaoyao Zhan,[*,‡,§] Liang Wang,[‡,§] Shuanglong Feng,[‡,§] Xiangyu Chai,[†] Wenqiang Lu,[*,‡,§] Jun Shen,[‡,§] Zhankun Weng,[*,†] and Jie Sun[∥]

[†]School of Electronics and Information Engineering, Changchun University of Science and Technology, 7089 Weixing Road, Changchun, Jilin 130022, People's Republic of China

[‡]Chongqing Institute of Green and Intelligent Technology, Chinese Academy of Sciences, Chongqing, 400714, People's Republic of China

[§]Chongqing Key Laboratory of Multi-scale Manufacturing Technology, Chongqing Institute of Green and Intelligent Technology, Chinese Academy of Sciences, Chongqing 400714, People's Republic of China

[∥]College of Electronic Information and Control Engineering, Beijing University of Technology, 100 Ping Le Yuan, Chaoyang District, Beijing 100124, People's Republic of China

Supporting Information

ABSTRACT: Catalyst-free, selective growth of ZnO nanowires directly on the commonly used dielectric SiO_2 layer is of both scientific significance and application importance, yet it is still a challenge. Here, we report a facile method to grow single-crystal ZnO nanowires on a large scale directly on SiO_2/Si substrate through vapor−solid mechanism without using any predeposited metal catalyst or seed layer. We found that a rough SiO_2/Si substrate surface created by the reactive ion etching is critical for ZnO growth without using catalyst. ZnO nanowire array exclusively grows in area etched by the reactive ion etching method. The advantages of this method include facile and safe roughness-assisted catalyst-free growth of ZnO nanowires on SiO_2/Si substrate and the subsequent transfer-free fabrication of electronic or optoelectronic devices. The ZnO nanowire UV photodetector fabricated by a transfer-free process presented high performance in responsivity, quantum efficiency and response speed, even without any post-treatments. The strategy shown here would greatly reduce the complexity in nanodevice fabrication and give an impetus to the application of ZnO nanowires in nanoelectronics and optoelectronics.

KEYWORDS: *catalyst-free, transfer-free, ZnO nanowires, UV photodetector*

1. INTRODUCTION

ZnO is a low cost, environmentally benign, intrinsically *n*-type semiconductor with amazing electronic, optical, mechanical, and biocompatible properties.[1] Owing to the large surface-to-volume ratio; good tunability in electronic,[2,3] optical,[4,5] mechanical[6] and even magnetic[7] properties; and fast charge transport,[8] ZnO nanowires have long been considered as competitive candidates for the building blocks of future nanoelectronic devices. In the last two decades, ZnO nanowires have been extensively exploited for sensing or detecting various of different physical phenomena such as typical nanoelectronic devices,[5,9−11] various kinds of sensors,[2,3,10,12−22] dilute magnetic semiconductor,[23,24] and ultraviolet (UV) photodetectors.[25−28] Meanwhile, UV photodetection is of great importance for various applications including environmental and biological research, sensing, detection, and missile launch.[29] To fully fulfill the potential in UV photodetection, a direct and transfer-free integration of ZnO nanowires into UV photodetectors at a relatively low cost, is highly desirable and is still a challenge due to the limited capability of existing ZnO nanowire preparation methods.

Various techniques have been developed to grow ZnO nanowires. These techniques include chemical reactions from aqueous solutions and chemical vapor deposition (CVD) via vapor−liquid−solid (VLS) or vapor−solid (VS) growth mechanisms. The chemical reaction method in aqueous solution needs a predeposited seed layer, and the aqueous environment tends to produce very short ZnO nanowires with low crystallinity, which is not suitable for high performance UV photodetectors fabrication.[30−32] To grow high-crystallinity

Received: June 30, 2015
Accepted: August 26, 2015
Published: August 26, 2015

DOI: 10.1021/acsami.5b05811
ACS Appl. Mater. Interfaces 2015, 7, 20264−20271

ZnO nanowires, we always employed high-temperature methods. In general, growth of nanowires at high temperature is conducted on Si substrate coated a layer of gold film as catalyst;[1,4,27,33] which really achieves good control in crystallinity and dimension of the ZnO nanowires, but the ZnO nanowires grown on Si substrate need to be transferred onto another dielectric layer such as SiO_2 before fabricating electronic devices, because the ZnO nanowires are directly connected to the Si substrate after growth. In addition, the use of metal catalysts tends to contaminate the final products, and the catalyst droplets at the growing end of the nanowires will also affect the performance of the ZnO nanowire nanodevices.[34,35] Therefore, direct growth of ZnO nanowires on a common dielectric layer, such as SiO_2, with CVD method is of great significance and enables a direct integration of ZnO nanowires with the most commonly used dielectric layer without the after-growth transfer. Nevertheless, direct, selective growth of ZnO nanowires on SiO_2 is still a challenge, though it has also been achieved by thermal evaporation of zinc powder or a mixture of ZnO and graphite powders via a VS growth mechanism.[18,36] However, these methods are suffering the low growth rate and low control in dimension and morphology of the final product, complicating the subsequent device fabrication process. Thus, developing catalyst-free CVD method for high-quality ZnO nanowires synthesis is extremely desirable.

Ho et al. have developed a roughness-assisted, catalyst-free method to grow ZnO nanowires on various substrates, including sapphire, glass, Si; mechanical scratch, mechanical polishing, and wet chemical etching were employed to roughen these substrates by using steel needles, abrasive papers, and sodium hydroxide solution, respectively.[37,38] However, the mechanical scratch and polishing were not suitable for processing arbitrary area (large, small, or patterned area); in addition, hard substrates require even harder tools. Among all the methods proposed by them, the wet-chemical method may be the only one that could realize arbitrary patterned surface processing.[37] To selectively roughen arbitrary areas on the most widely used SiO_2/Si substrates, we employed wet-chemical etching with HF solution, which is extremely dangerous and inconvenient in practical application. Here, we report a novel method to realize catalyst-free growth of ZnO nanowires directly on SiO_2/Si substrate by CVD method. A facile surface treatment on SiO_2/Si substrate by reactive ion etching (RIE) is essential for the ZnO nanowires growth. It is believed that the large lattice mismatch between ZnO and SiO_2 makes the ZnO nucleation on SiO_2 very difficult; RIE on SiO_2 will create a rough surface and also a large amount of dangling bonds, facilitating ZnO nanowires nucleation and growth. Combined with a standard lithographic process, RIE enables ZnO nanowires array to exclusively grow in the etched area of arbitrary patterns. Compared with reported catalyst-free growth of ZnO nanowires on SiO_2/Si substrates, this strategy is much simpler, safer, cheaper, and more controllable.[18,38−42] The as-grown ZnO nanowires on SiO_2/Si could be directly fabricated into UV photodetectors by depositing metal contact electrodes without being transferred to other dielectric layers. The present study demonstrates a simple but effective method to grow ZnO nanowires on SiO_2/Si substrates, which have been thought to be difficult or impossible. The strategy shown here would greatly reduce the complexity in nanodevice fabrication processes and improve the application of ZnO nanostructures in nanoelectronics and optoelectronics.

2. EXPERIMENTAL METHODS

2.1. RIE on SiO_2/Si substrates. P typed Si wafers with approximate 500 nm SiO_2 were used as the substrates for ZnO nanowires synthesis. The SiO_2/Si wafers were first cleaned with acetone and Isopropanol (IPA) in sequence with the help of ultrasound, and then the wafers were dried with nitrogen gun. The RIE was conducted in RIE system (ME-3A, IMC, CAS, Beijing), with CHF_3 as etchant, the flow rate was set to 40 sccm, and the radio frequency (RF) power was set to 100 W with a bias voltage of 390 V. After surface treatment, the etched wafers were rigidly washed with acetone and IPA several times to remove the residuals. Arbitrary patterns could also be etched with the help of a standard lithographic process. The depth of etched SiO_2 was inspected by white light interferometer, and the surface morphology of the etched substrate was characterized by atomic force microscopy (AFM, Bruker Dimension Edge).

2.2. CVD Growth of ZnO Nanowires. The CVD growth of ZnO nanowires were conducted in a tube furnace with inner diameter of 2 in. In a typical synthesis procedure, a mixture of ZnO powder and micron-sized diamond power[43] with a weight ratio of 3:1 was used as the raw material, which was placed in an alumina boat. SiO_2/Si substrates (1×1 cm^2) were laid on the alumina boat with the etched SiO_2 side facing the source to collect products. Then, the alumina boat with source and SiO_2/Si substrates was placed at the center of a quartz tube inserted in a horizontal tube furnace. N_2 gas was introduced at a flow rate of 100 sccm into the quartz tube as the carrier gas; the pressure in the quartz tube was adjusted to 30 kpa. The temperature was ramped to 960 °C at a rate of 15 °C/min, and 1.5 sccm oxygen was introduced into the tube at 600 °C. The furnace was kept at 960 °C for 30 min, and then the oxygen was switched off and the furnace was cooled naturally down to room temperature. After growth, a layer of white or gray matters were obtained on the SiO_2/Si substrates.

2.3. Characterizations. The morphology and crystal structure of the as-grown ZnO nanowires were characterized by field emission scanning electron microscope (FESEM, JEOL7600), high-resolution transmission electron microscopy (HRTEM, JEM2100 operated at 200 kV, JEOL), and X-ray diffractometer (XRD) (Rigaku RINT2500 TRAX−III, Cu Kα radiation). Raman scattering of the as-grown ZnO nanowires were collected on a Ranishaw inVia Raman microscope with an excitation laser of 514 nm.

2.4. UV Photodetectors Fabrication and Testing. To fabricate the metal−semiconductor−metal structured ZnO Nanowire UV photodetectors, silver paint was applied onto the top surface of the ZnO nanowires array to form two Ag electrodes with internal space around 4 mm and enough thickness. Photoresponse tests were performed on an electrochemical workstation (CHI 660D). The sampling period was set to 10 ms, and the change in current of the UV photodetector with or without light illumination was recorded by the electrochemical workstation. A 400 W xenon lamp with an output window diameter of 10 cm was adopted as the light source, and the UV power density incident to the device surface is estimated to be 14 mW cm^{-2}. The "on" and "off" of the illumination were controlled by a chopper. All of the above measurements were conducted in a dark room to minimize the influence of natural light.

3. RESULTS AND DISCUSSION

3.1. ZnO Nanowire Characterization. The schematic diagram of the growth process is shown in Figure 1. A clean SiO_2/Si substrate was first etched using RIE to create rough surface that was full of spikes and valleys, as displayed in Figure 1b. Then the etched SiO_2/Si substrate was loaded into the furnace to start the growth. At the first stage, the ZnO_x nanoclusters would first form and serve a nucleation sites for the subsequent ZnO nanowires growth (see Figure 1c); then ZnO nanowires sprouted from the nuclei as shown in Figure 1d.

The obtained ZnO nanowires on the etched SiO_2/Si substrate can be seen in Figure 2a. The nanowire array has a

DOI: 10.1021/acsami.5b05811
ACS Appl. Mater. Interfaces 2015, 7, 20264−20271

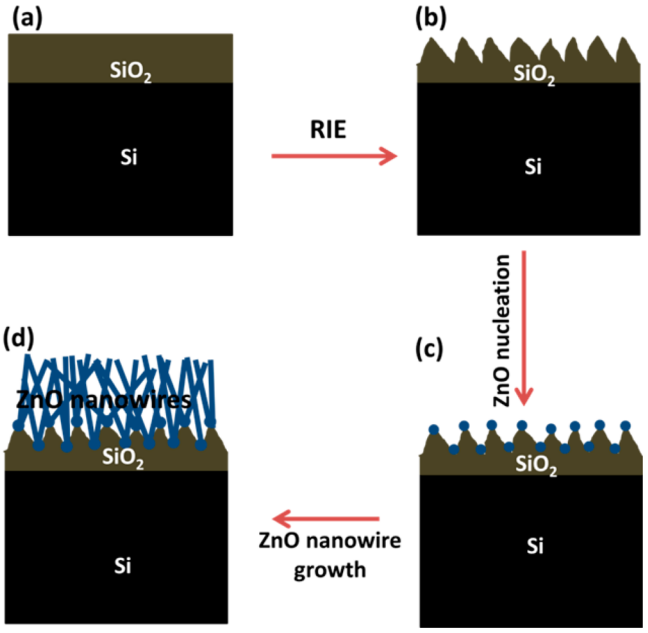

Figure 1. Schematic diagram of the growth process of ZnO nanowire array on RIE etched SiO_2/Si. (a) Flat and smooth pristine SiO_2/Si substrate before RIE etching; (b) Roughened SiO_2/Si substrate surface after RIE etching; (c) ZnO nucleation on the RIE etched SiO_2/Si substrate; (d) ZnO nanowires grown from the ZnO nuclei.

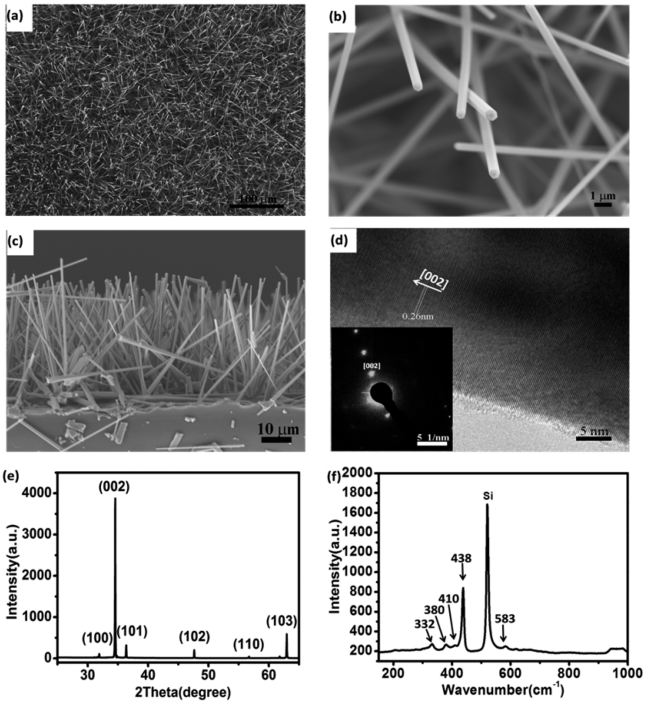

Figure 2. Characterization on ZnO nanowires grown on RIE etched SiO_2/Si by a catalyst-free CVD method. (a) SEM image of the ZnO nanowires array; (b) SEM of ZnO nanowires with clean and hexagonal tips; (c) SEM image of side view of a ZnO nanowire array; (d) HRTEM image of a single ZnO nanowire with the adjacent fringe distance of 0.26 nm and the growth direction in [001], inset is the corresponding SAED pattern of the ZnO nanowire indicating the growth direction is [001]; (e) XRD patterns of the obtained ZnO nanowires on SiO_2/Si; (f) Raman spectrum of the ZnO nanowire array on SiO_2/Si substrate.

high density, as individual nanowires entangle with each other, which will be beneficial for UV photodetector fabrication. Figure 2b presents an enlarged SEM image of several ZnO nanowire tips, showing that there are no metal catalyst particles on the nanowire tips, indicating the growth mechanism to be a vapor−solid (VS) mechanism. In addition, a very regular hexagonal cross-section of ZnO nanowire tip implicates that the obtained ZnO nanowires grow along the highly symmetrical direction of [001], as shown in Figure S1 (Supporting Information). Figure 2c shows a side view of a typical ZnO nanowire array grown on SiO_2/Si substrate, suggesting that the ZnO nanowires could reach around 40 μm in length after 30 min growth. It is interesting to observe that the VS process is also able to grow ultralong aligned nanowires at a high growth rate, which is another beneficial asset to VS growth. Normally, ZnO nanowires grown by a VS process are believed to have a lower growth rate than that of VLS processes owing to lower surface diffusion on solid surface.[44] A high-resolution TEM image of one single ZnO nanowire is displayed in Figure 2d. The spacing of 2.6 Å between adjacent fringes corresponds to the distance between two (002) crystal planes, indicating that the [001] is the preferential growth direction for the ZnO nanowires, the inset selected area electron diffraction (SAED) image also confirms the single crystallinity and growth direction of [001] for ZnO nanowires.

XRD patterns of ZnO nanowire samples were taken to study the crystallographic information on the nanowires. All samples gave similar XRD patterns, indicating high reproducibility of this method. Figure 2e shows a typical XRD pattern of the ZnO nanowires, the diffraction peaks can be indexed to a hexagonal structure of bulk ZnO with cell constants of a = 3.24 Å and c = 5.2 Å. Judging from the XRD pattern, there is not any impurity pattern could be observed, which is opposite to the catalyst-assisted grown ZnO nanowires.[33] The prominent diffraction of (002) peaks in Figure 2e is also a manifest of preferential growth direction [001]. All these observations confirm that the obtained products are single-crystal ZnO nanowires with a preferential growth direction of [001]. Raman spectroscopy was also utilized to examine the fine structure of the ZnO nanowires. Figure 2f shows a Raman spectrum of the ZnO nanowires in the wavenumber range from 150 to 1000 cm^{-1}. Four first-order Raman-active phonon bands of wurtzite structure ZnO are observed. The most prominent peak at 438 cm^{-1} corresponds to nonpolar optical phonon E_2 (high) of wurtzitic ZnO, and it is a fingerprint of hexagonal phase ZnO. The peaks at 380 and 410 cm^{-1} agree well with A_1 (TO) and E_1 (TO) phonon modes of wurtzite ZnO, respectively. The band 583 cm^{-1} is assigned to the E_1 (LO) mode of hexagonal ZnO, which is associated with oxygen deficiency. The Raman mode at 332 cm^{-1} is indexed to the second-order Raman vibration mode arising from zone-boundary phonons of hexagonal ZnO. All these data agree well with reported investigations on Raman spectra of wurtzite structure ZnO crystals.[45]

3.2. Growth Mechanism Study. To investigate the role of RIE on SiO_2/Si substrates in the growth of ZnO nanowires, a set of patterns were intentionally fabricated on SiO_2/Si substrates with help of standard lithograph and subsequent RIE dry etching. Under our RIE condition, the etch rate of SiO_2 is around 60 nm/min. Figure 3a shows a 3D white light interferometry image of CIGIT patterns after 5 min of etching; and the blue areas correspond to the trench structures created by RIE process. Figure 3b shows the corresponding depth profile of the etched CIGIT patterns, and the depth of these

DOI: 10.1021/acsami.5b05811
ACS Appl. Mater. Interfaces 2015, 7, 20264−20271

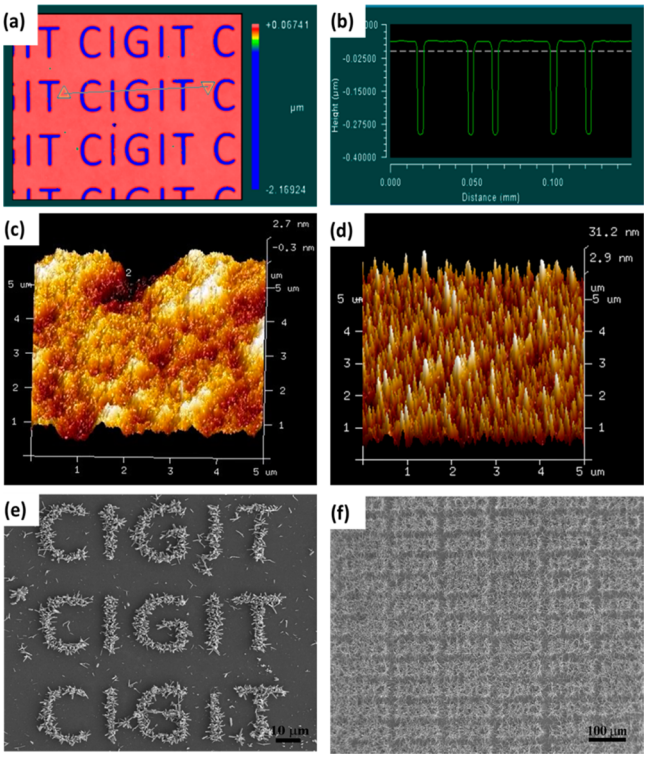

Figure 3. (a) 3D white light interferometry image of CIGIT patterns fabricated by 5 min RIE etch; (b) corresponding depth profile of the etched CIGIT patterns in panel a; (c and d) 3D AFM images of original and RIE etched SiO_2/Si substrate surface respectively; (e and f) SEM image of ZnO nanowires grown on RIE etched CIGIT logo patterns at initial growth stage and after 30 min of growth, respectively.

etched patterns is around 300 nm. We further examined the critical effect of RIE on ZnO nanowires growth on the SiO_2/Si substrate. AFM was employed to measure the surface morphology of SiO_2/Si substrate surface before and after RIE. Figure 3c shows the AFM image of SiO_2/Si substrate before etching, the surface was very flat with a roughness value of around 0.7 nm. As expected, after being etched for 5 min, the SiO_2/Si surface became much rougher, with the roughness value soaring to 7.9 nm, as displayed in Figure 3d. The morphology of ZnO nanowires at initial stage of growth is shown in Figure 3e, It can be found that only the roughened areas (etched areas) favor growth of ZnO nanowires in our experiments, and almost no ZnO nanowire growth happens in the intact area, indicating the crucial role of the etched SiO_2/Si surface for growth of ZnO nanowires. It can be found in Figure 3f, after 30 min of reaction, the ZnO nanowires grow to tens of microns in length and tend to entangle with each other, resulting in blurred boundaries between different patterns.

The effect of surface roughness on the ZnO growth was also investigated. The AFM images of SiO_2/Si substrates that were etched for varied time were presented in Figure S2 (Supporting Information). The evolution of substrate surface morphology with time suggests that substrate surface become rougher with the ecth time (Figure S2a–c, Supporting Information), the detailed relationship between the roughness value and etching time in Figure S2d (Supporting Information), is synnonymous to the morphology evolution, suggesting that at a fixed etch rate, the roughness is drastically increasing with the etching time. Though we measured the etch rate in our condition is around 60 nm/min, however, after 10 min etching, the SiO_2 layer has not been etched through. This could be well explained by the mechanism of surface roughning by RIE process. During the RIE processing; both volatile and nonvolatile species will be formed. The nonvolatile residuals on the surface will shield surface atoms from reaction with incoming ions and serve as "micromasks" that shadow regions of the surface and can lead to spike and valley structures on the surface as the etch process continues. The accumulation of these "micromasks" would also decrease the overall etch rate.[46] The etched substrates were then used to grow ZnO nanowires. As expected, in our growth condition, there was almost no ZnO nanowire growing on the flat SiO_2/Si substrate (Figure 4a), which reconciled with

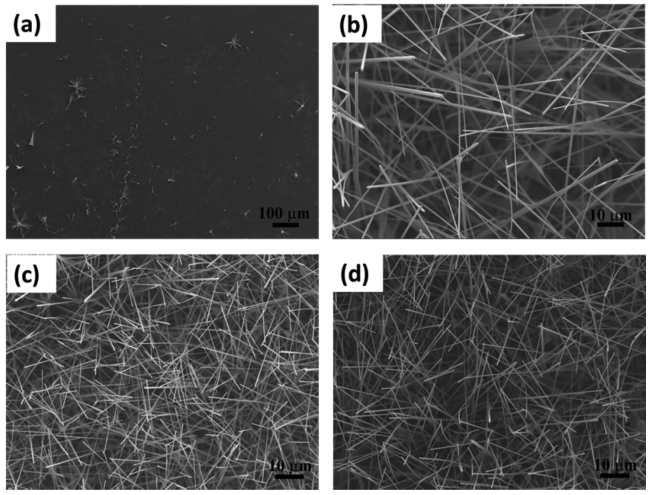

Figure 4. SEM images of ZnO nanowires grown on SiO_2/Si substrates that were etched for different periods: (a) 0, (b) 1, (c) 5, and (d) 10 min.

observation in Figure 3e,f, indicating the critical role of RIE treatment; the substrates became reactive for ZnO nanowire growth by RIE processing. SEM images in Figure 4b–d suggested that the morphology of ZnO nanowires grown on substrates that were etched for 1, 5, and 10 min, were also highly similar, except there was a slight difference in nanowire density, which is highest for 5 min etching; the reason is still under investigating.

Because no catalyst was coated on the substrate before the growth or catalyst particle on the tip of ZnO nanowires after growth, as shown in Figure 2b and Figure S1 (Supporting Information), thus a VS growth mechanism dominated instead of VLS process which is widely utilized to grow aligned nanowire arrays. The process of the catalyst-free ZnO nanowires growth on RIE processed SiO_2/Si substrate is as shemetically discribed in Figure 1. The detailed process of catalyst-free growth of ZnO nanowire on SiO_2 substrate is still not well understood, because of the large lattice mismatch between ZnO and SiO_2. We try to examine the ZnO morphologies at the beginning of growth and after 10 min growth. As opposed to a flat surface, we can see that small nanoclusters were formed in the etched area before ZnO nanowires sprouted from the nanoclusters, (Figure S3a, Supporting Information). After 10 min growth, ZnO nanowires come out from the nanoclusters and extend to more than 10 μm in length, as shown in figure S3b(see Supporting Information). However, we failed to capture the SEM image of ZnO nuclei that were just formed at spike or valley sites. Because the temperature ramping from 600 to 960 °C will take

DOI: 10.1021/acsami.5b05811
ACS Appl. Mater. Interfaces 2015, 7, 20264–20271

around 30 min (determined by the power of furnace), it is very difficult to determine the exact moment at which the ZnO just nucleate at spike/valley sites.

We speculate that ZnO nucleation would preferentially take place at the tiny spikes/valleys, because the etched area on SiO_2/Si substrate is full of spikes and valleys(as shown in Figure S2a-c in Supporting Information), meanwhile, there are also a great deal of highly reactive dangling bonds created by the etching and ion bombarding in the etched area.[47] The Zn vapor generated by carbothermal reduction of ZnO power source will be trapped in the rough etched area (as shown in Figure 1c), because of higher energy barrier for Zn species migration at spike/valley sites,[37] in addition, the dangling bonds on these etched sites are extremely reactive and will bind with the adsorbed Zn atoms to form clusters, the subsequent reaction of Zn clusters with oxygen results in the formation of ZnO_x wetting layer, which serve as nucleation sites.[48] The continuous impinging of Zn and O_2 promotes the growth of individual solid ZnO nanowires on the available nuclei sites.

3.3. Photoresponsive Behavior of ZnO Nanowire UV Photodetector. The direct, catalyst-free growth of ZnO nanowires on dielectric SiO_2 layer enables fabrication of electronic and optoelectronic devices directly on this commonly used dielectric substrate without using after-growth transfer processes. As shown in Figure 5a, metal electrodes could be directly fabricated through screen printing or shadow-mask assisted deposition method onto the as-obtained ZnO nanowire arrays. In our experiment, silver paint was directly applied onto ZnO nanowire arrays to form the electrodes. The optical image of a typical device is shown in Figure 5b; the active area of the device is around 4 × 1 mm^2. The photoresponse tests were conducted in a dark environment to exclude the effect of natural light; the "on" and "off" of UV illumination were controlled by a metal chopper. The photoresponse to UV illumination are shown in Figure 5c–f. Figure 5c shows $I-V$ characteristic curves of the ZnO nanowires photodetector with and without light illumination. The dark current is around 100 μA under a bias of 5 V, and jumps to around 400 μA under a bias of 5 V. It is obvious that the UV illumination could significantly enhance the conductivity of the nanowire device. The asymmetrical $I-V$ transport curve indicated Schottky contacts at two electrodes.[49] The high dark current should be a result of direct connection between ZnO nanowire and Si substrate at the edge of substrate (see Figure 2c). The dark current could be greatly reduced by defining the ZnO nanowire growth area in a smaller area at the interior part of the substrate surface through RIE dry etching, and ZnO nanowires could merely grow in the etched area with a clear peripheral margin along the edge of substrate. We have estimated the density and length of ZnO nanowires on the substrates to be 0.1/μm^2 and 40 μm, respectively. The active device size is around 4 × 1.0 mm^2. Thus, there are around 6 × 10^5 nanowires in the active area of the device. The responsivity (R) is defined as the ratio of the response current to the illumination power on photodetector as given by

$$R = \frac{I_{ph}}{P_o A} \tag{1}$$

where I_{ph} is the photocurrent (current increment by the UV illumination), P_o *is* the incident UV power density, and A is the active device area. In our experiment, the UV illumination power density is 14 mW/cm^2, the active area is 4 mm^2, and we can obtain R = 0.5 A/W.

The external quantum efficiency (EQE) of the photodetector is defined as the number of charge carriers generated per number of incident photons on the device as given by the following relation:

$$\mathrm{EQE} = \frac{R}{(h\nu/q)} \tag{2}$$

where h is Planck's constant, ν is the frequency of incident light, and q is the elemental charge. We used wavelength of 365 nm (UV is not purely monochromatic) to calculate the EQE, thus we estimated the EQE of 160%. The device performance could be comparable with those of reported pure ZnO nanostructures based UV photodetectors.[50,51] Both the responsivity and EQE could be improved by optimizing the density of ZnO nanowires and simple thermal annealing in oxygen-rich environment. Please note that the ZnO nanowires are grown in an oxygen deficient environment and thus have a great deal of oxygen vacancies, a simple thermal treatment in oxygen or hydrogen could greatly reduce the defects amount.[30−32] In addition, the density of ZnO nanowires grown under current condition is still very low, and could be improved by optimizing the growth condition.

The response time is another important indicator of merit of a photodetector. To examine the response time of the ZnO nanowires UV photodetector, the time-dependent photocurrent at 5 V bias with multiple UV on/off cycles was

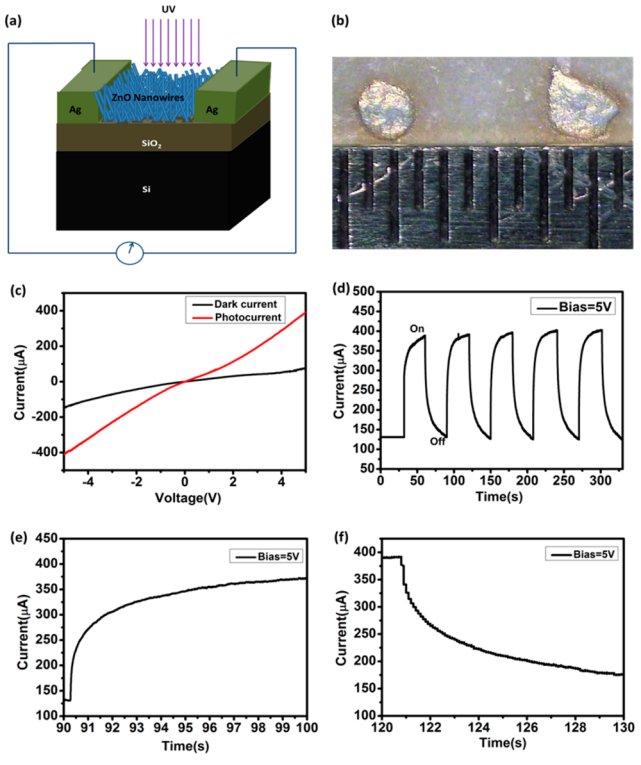

Figure 5. Photoresponse behavior of ZnO nanowires UV photodetector. (a) Schematic of device structure and experimental setup; (b) optical image of a typical fabricated photodetector; (c) $I-V$ transport curves of the ZnO nanowires UV photodetector with UV illumination on and off; (d) time-resolved photocurrent rise and decay with UV illumination on and off periods of 30 s; (e and f) typical rise and decay curve for ZnO nanowires photodetector under illumination on and off, respectively.

DOI: 10.1021/acsami.5b05811
ACS Appl. Mater. Interfaces 2015, 7, 20264−20271

measured, in which both the "on" and "off" times of the UV illumination are 30 s. It is well-known oxygen molecules absorbed at surface of ZnO acting as electron acceptors to form O_2^- by capturing free electrons from the surface of ZnO in dark and create a low conductive depletion layer near the ZnO surface. Upon UV illumination, the photogenerated holes in ZnO migrate to the surface and neutralize the O_2^- ions, while the unpaired electrons significantly enhance the conductivity of the sample.[26,28,52] As shown in Figure 5d, upon UV illumination, the current would first rapidly ramp to 300 μA from the dark current, followed by a slow increase to around 400 μA; and as UV illumination is off, the current would first promptly fall to 230 μA and then slowly decay to around the original level. These observed time-resolved photocurrent course could be described by a fast photoresponse process followed by a slow one, and the latter one is governed by the low rate of the turnover of oxygen chemisorption/desorption on the ZnO surface. The dependence of both rise and decay of photocurrent on time could be well described by second-order decay functions as follows:[20]

$$y = y_0 + A_1 e^{(t/t_1)} + A_2 e^{(t/t_2)} \quad (3)$$

where, y_0, A_1, and A_2 are constants, t_1 and t_2 are time constants.

Figure 5e,f shows a typical rise and decay stage of the time-resolved photocurrent variation curve, respectively. By fitting the photocurrent data with the time, we estimated the time constants for rise stage are t_{r1} = 0.59 s, t_{r2} = 6.2 s, with relative weight factors of 65 and 34% respectively; while the time constants for decay stage are t_{d1} = 1s, t_{d2} = 10.1 s, with relative weight factors of 45 and 55%, respectively. The photoresponse speed is comparable with or higher than most reported photodetectors based on pure ZnO nanostructures,[20,26,53,54] though no post-treatment was conducted on ZnO nanowires. We expected that the performance of our ZnO nanowire photodetectors could be further improved by employing thermal annealing,[32,55] plasmonic nanoparticles modification,[50,54] heterojunction creation,[20] and so on. For the rise stage, the fast process is a result of photocarriers generation excited by UV illumination, however, the slow one is governed by readsorption of oxygen molecules on ZnO surface; when the UV illumination is off, the fast decay process is related to photocarrier recombination, and the slow one is controlled by the slow physisorption of oxygen molecules.[53]

4. CONCLUSION

In summary, we demonstrated that single-crystal ZnO nanowire array could be exclusively grown on RIE etched SiO_2/Si substrate without predeposited catalyst or seed-layer. A roughened SiO_2/Si substrate surface could be created by a simple RIE process, which favors the growth of ZnO nanowires on the SiO_2/Si substrate through a VS mechanism. The advantages of this method include facile and safe achievement of the growth of ZnO nanowires on SiO_2/Si substrate; and of the subsequent transfer-free fabrication of electronic or optoelectronic devices. The ZnO nanowire UV photodetector fabricated by a transfer-free process presented high performance in responsivity, EQE and response speed, even without any post-treatments. The strategy shown here would greatly reduce the complexity in nanodevice fabrication processes and significantly prompt the application of ZnO nanostructures in nanoelectronics and optoelectronics.

ASSOCIATED CONTENT

Supporting Information

The Supporting Information is available free of charge on the ACS Publications website at DOI: 10.1021/acsami.5b05811.

Additional SEM image of individual ZnO nanowire, AFM images of SiO_2/Si substrates that were etched for different periods, and SEM images of ZnO nanowires grown on CIGIT logo at different growth stages. (PDF)

AUTHOR INFORMATION

Corresponding Authors

*E-mail: zhanhit@hotmail.com.
*E-mail: wqlu@cigit.ac.cn.
*E-mail: wengzk@cust.edu.cn.

Notes

The authors declare no competing financial interest.

ACKNOWLEDGMENTS

This work was supported by National Natural Science Foundation of China (No. 51402290) and the Beijing Natural Science Foundation (No. 4152003).

REFERENCES

(1) Wang, Z. L. Zinc Oxide Nanostructures: Growth, Properties and Applications. *J. Phys.: Condens. Matter* **2004**, *16*, R829−R858.
(2) Xue, F.; Zhang, L. M.; Tang, W.; Zhang, C.; Du, W. M.; Wang, Z. L. Piezotronic Effect on ZnO Nanowire Film Based Temperature Sensor. *ACS Appl. Mater. Interfaces* **2014**, *6*, 5955−5961.
(3) Jiang, C.; Song, J. Significant Photoelectric Property Change Caused by Additional Nano-Confinement: A Study of Half-dimensional Nanomaterials. *Small* **2014**, *10*, 5042−5046.
(4) Yang, P. D.; Yan, H. Q.; Mao, S.; Russo, R.; Johnson, J.; Saykally, R.; Morris, N.; Pham, J.; He, R. R.; Choi, H. J. Controlled Growth of ZnO Nanowires and Their Optical Properties. *Adv. Funct. Mater.* **2002**, *12*, 323−331.
(5) Ju, S. Y.; Facchetti, A.; Xuan, Y.; Liu, J.; Ishikawa, F.; Ye, P. D.; Zhou, C. W.; Marks, T. J.; Janes, D. B. Fabrication of Fully Transparent Nanowire Transistors for Transparent and Flexible Electronics. *Nat. Nanotechnol.* **2007**, *2*, 378−384.
(6) Jiang, C.; Lu, W.; Song, J. Shear Modulus Property Characterization of Nanorods. *Nano Lett.* **2013**, *13*, 111−115.
(7) Lee, J. J.; Xing, G. Z.; Yi, J. B.; Chen, T.; Ionescu, M.; Li, S. Tailoring the Coercivity In Ferromagnetic ZnO Thin Films by 3d and 4f Elements Codoping. *Appl. Phys. Lett.* **2014**, *104*, 012405.
(8) Law, M.; Greene, L. E.; Johnson, J. C.; Saykally, R.; Yang, P. D. Nanowire Dye-sensitized Solar Cells. *Nat. Mater.* **2005**, *4*, 455−459.
(9) Huang, H. T.; Liang, B.; Liu, Z.; Wang, X. F.; Chen, D.; Shen, G. Z. Metal Oxide Nanowire Transistors. *J. Mater. Chem.* **2012**, *22*, 13428−13445.
(10) Wang, X. D.; Summers, C. J.; Wang, Z. L. Large-Scale Hexagonal-patterned Growth of Aligned ZnO Nanorods for Nano-optoelectronics and Nanosensor Arrays. *Nano Lett.* **2004**, *4*, 423−426.
(11) Ng, H. T.; Han, J.; Yamada, T.; Nguyen, P.; Chen, Y. P.; Meyyappan, M. Single Crystal Nanowire Vertical Surround-gate Field-effect Transistor. *Nano Lett.* **2004**, *4*, 1247−1252.
(12) Fulati, A.; Usman Ali, S. M.; Riaz, M.; Amin, G.; Nur, O.; Willander, M. Miniaturized pH Sensors Based on Zinc Oxide Nanotubes/Nanorods. *Sensors* **2009**, *9*, 8911−8923.
(13) Wang, X. D.; Zhou, J.; Song, J. H.; Liu, J.; Xu, N. S.; Wang, Z. L. Piezoelectric Field Effect Transistor and Nanoforce Sensor Based on a Single ZnO Nanowire. *Nano Lett.* **2006**, *6*, 2768−2772.
(14) Jiang, C.; Tang, C.; Song, J. The Smallest Resonator Arrays in Atmosphere by Chip-Size-Grown Nanowires with Tunable Q-factor and Frequency for Subnanometer Thickness Detection. *Nano Lett.* **2015**, *15*, 1128−1134.

DOI: 10.1021/acsami.5b05811
ACS Appl. Mater. Interfaces 2015, 7, 20264−20271

(15) Liu, X. H.; Zhang, J.; Wang, L. W.; Yang, T. L.; Guo, X. Z.; Wu, S. H.; Wang, S. R. 3D Hierarchically Porous ZnO Structures and Their Functionalization by Au Nanoparticles for Gas Sensors. *J. Mater. Chem.* **2011**, *21*, 349−356.
(16) Park, S.; An, S.; Ko, H.; Jin, C.; Lee, C. Synthesis of Nanograined ZnO Nanowires and Their Enhanced Gas Sensing Properties. *ACS Appl. Mater. Interfaces* **2012**, *4*, 3650−3656.
(17) Yang, Y.; Qi, J. J.; Guo, W.; Gu, Y. S.; Huang, Y. H.; Zhang, Y. Transverse Piezoelectric Field-effect Transistor Based on Single ZnO Nanobelts. *Phys. Chem. Chem. Phys.* **2010**, *12*, 12415−12419.
(18) San, X. G.; Wang, G. S.; Liang, B.; Song, Y. M.; Gao, S. Y.; Zhang, J. S.; Meng, F. L. Catalyst-free Growth of One-dimensional ZnO Nanostructures on SiO2 Substrate and In Situ Investigation of Their H2 Sensing Properties. *J. Alloys Compd.* **2015**, *622*, 73−78.
(19) Liao, X. Q.; Yan, X. Q.; Lin, P.; Lu, S. G.; Tian, Y.; Zhang, Y. Enhanced Performance of ZnO Piezotronic Pressure Sensor through Electron-tunneling Modulation of MgO Nano Layer. *ACS Appl. Mater. Interfaces* **2015**, *7*, 1602−1607.
(20) Zhou, J.; Gu, Y.; Hu, Y.; Mai, W.; Yeh, P.-H.; Bao, G.; Sood, A. K.; Polla, D. L.; Wang, Z. L. Gigantic Enhancement in Response and Reset Time of ZnO UV Nanosensor by Utilizing Schottky Contact and Surface Functionalization. *Appl. Phys. Lett.* **2009**, *94*, 191103.
(21) Zhang, Y.; Xiang, Q.; Xu, J. Q.; Xu, P. C.; Pan, Q. Y.; Li, F. Self-Assemblies of Pd Nanoparticles on the Surfaces of Single Crystal ZnO Nanowires for Chemical Sensors with Enhanced Performances. *J. Mater. Chem.* **2009**, *19*, 4701−4706.
(22) Al-Hilli, S. M.; Willander, M.; Ost, A.; Stralfors, P. ZnO Nanorods as an Intracellular Sensor for pH Measurements. *J. Appl. Phys.* **2007**, *102*, 084304.
(23) Xing, G. Z.; Wang, D. D.; Cheng, C. J.; He, M.; Li, S.; Wu, T. Emergent Ferromagnetism in ZnO/Al2O3 Core-shell Nanowires: Towards Oxide Spinterfaces. *Appl. Phys. Lett.* **2013**, *103*, 022402.
(24) Wang, D. D.; Xing, G. Z.; Yan, F.; Yan, Y. S.; Li, S. Ferromagnetic (Mn, N)-codoped ZnO Nanopillars Array: Experimental and Computational Insights. *Appl. Phys. Lett.* **2014**, *104*, 022412.
(25) Leschkies, K. S.; Divakar, R.; Basu, J.; Enache-Pommer, E.; Boercker, J. E.; Carter, C. B.; Kortshagen, U. R.; Norris, D. J.; Aydil, E. S. Photosensitization of ZnO Nanowires with CdSe Quantum Dots for Photovoltaic Devices. *Nano Lett.* **2007**, *7*, 1793−1798.
(26) Kind, H.; Yan, H. Q.; Messer, B.; Law, M.; Yang, P. D. Nanowire Ultraviolet Photodetectors and Optical Switches. *Adv. Mater.* **2002**, *14*, 158−160.
(27) Soci, C.; Zhang, A.; Xiang, B.; Dayeh, S. A.; Aplin, D. P. R.; Park, J.; Bao, X. Y.; Lo, Y. H.; Wang, D. ZnO Nanowire UV Photodetectors with High Internal Gain. *Nano Lett.* **2007**, *7*, 1003−1009.
(28) Zhan, Z.; Zheng, L.; Pan, Y.; Sun, G.; Li, L. Self-Powered, Visible-Light Photodetector Based on Thermally Reduced Graphene Oxide-ZnO (rGO-ZnO) Hybrid Nanostructure. *J. Mater. Chem.* **2012**, *22*, 2589−2595.
(29) Monroy, E.; Omnes, F.; Calle, F. Wide-bandgap Semiconductor Ultraviolet Photodetectors. *Semicond. Sci. Technol.* **2003**, *18*, R33−R51.
(30) Greene, L. E.; Law, M.; Goldberger, J.; Kim, F.; Johnson, J. C.; Zhang, Y. F.; Saykally, R. J.; Yang, P. D. Low-temperature Wafer-scale Production of ZnO Nanowire Arrays. *Angew. Chem., Int. Ed.* **2003**, *42*, 3031−3034.
(31) Huang, X. H.; Tay, C. B.; Zhan, Z. Y.; Zhang, C.; Zheng, L. X.; Venkatesan, T.; Chua, S. J. Universal Photoluminescence Evolution of Solution-grown ZnO Nanorods with Annealing: Important Role of Hydrogen Donor. *CrystEngComm* **2011**, *13*, 7032−7036.
(32) Huang, X. H.; Zhan, Z. Y.; Pramoda, K. P.; Zhang, C.; Zheng, L. X.; Chua, S. J. Correlating the Enhancement of UV Luminescence from Solution-grown ZnO Nanorods with Hydrogen Doping. *CrystEngComm* **2012**, *14*, 5163−5165.
(33) Huang, M. H.; Wu, Y. Y.; Feick, H.; Tran, N.; Weber, E.; Yang, P. D. Catalytic Growth of Zinc Oxide Nanowires by Vapor Transport. *Adv. Mater.* **2001**, *13*, 113−116.
(34) Zhan, Z. Y.; An, J. N.; Zhang, H. C.; Hansen, R. V.; Zheng, L. X. Three-dimensional Plasmonic Photoanodes Based on Au-embedded TiO2 Structures for Enhanced Visible-light Water Splitting. *ACS Appl. Mater. Interfaces* **2014**, *6*, 1139−1144.
(35) Cheng, C. W.; Sie, E. J.; Liu, B.; Huan, C. H. A.; Sum, T. C.; Sun, H. D.; Fan, H. J. Surface Plasmon Enhanced Band Edge Luminescence of ZnO Nanorods by Capping Au Nanoparticles. *Appl. Phys. Lett.* **2010**, *96*, 071107.
(36) Kim, H. J.; Park, S. H.; Lee, W. J.; Bae, J. M.; Chae, J. M.; Cho, M. H. Temperature-dependent Catalyst-free Growth of ZnO Nanostructures on Si and SiO2/Si Substrates via Thermal Evaporation. *J. Korean Phys. Soc.* **2012**, *60*, 1877−1885.
(37) Ho, S. T.; Wang, C. Y.; Liu, H. L.; Lin, H. N. Catalyst-Free Selective-area Growth of Vertically Aligned Zinc Oxide Nanowires. *Chem. Phys. Lett.* **2008**, *463*, 141−144.
(38) Ho, S.-T.; Chen, K.-C.; Chen, H.-A.; Lin, H.-Y.; Cheng, C.-Y.; Lin, H.-N. Catalyst-free Surface-roughness-assisted Growth of Large-scale Vertically Aligned Zinc Oxide Nanowires by Thermal Evaporation. *Chem. Mater.* **2007**, *19*, 4083−4086.
(39) Lu, W.; Jiang, C.; Caudle, D.; Tang, C.; Sun, Q.; Xu, J.; Song, J. Controllable Growth of Laterally Aligned Zinc Oxide Nanorod Arrays on a Selected Surface of the Silicon Substrate by a Satalyst-Free Vapor Solid Process - a Technique for Growing Nanocircuits. *Phys. Chem. Chem. Phys.* **2013**, *15*, 13532−13537.
(40) Lee, W.; Jeong, M. C.; Myoung, J. M. Catalyst-Free Growth of ZnO Nanowires by Metal-organic Chemical Vapor Deposition (MOCVD) and Thermal Evaporation. *Acta Mater.* **2004**, *52*, 3949−3957.
(41) Ham, H.; Shen, G. Z.; Cho, J. H.; Lee, T. J.; Seo, S. H.; Lee, C. J. Vertically Aligned ZnO Nanowires Produced by a Catalyst-free Thermal Evaporation Method and Their Field Emission Properties. *Chem. Phys. Lett.* **2005**, *404*, 69−73.
(42) Park, W. I.; Yi, G. C.; Kim, M. Y.; Pennycook, S. J. ZnO Nanoneedles Grown Vertically on Si Substrates by Non-catalytic Vapor-Phase Epitaxy. *Adv. Mater.* **2002**, *14*, 1841−1843.
(43) Li, H.-D.; Lu, H.; Sang, D.-D.; Li, D.-M.; Li, B.; Lue, X.-Y.; Zou, G.-T. Synthesizing of ZnO Micro/Nanostructures at Low Temperature with New Reducing Agents. *Chin. Phys. Lett.* **2008**, *25*, 3794−3797.
(44) Ramgir, N. S.; Subannajui, K.; Yang, Y.; Grimm, R.; Michiels, R.; Zacharias, M. Reactive VLS and The Reversible Switching between VS and VLS Growth Modes for ZnO Nanowire Growth. *J. Phys. Chem. C* **2010**, *114*, 10323−10329.
(45) Damen, T. C.; Porto, S. P. S.; Tell, B. Raman Effect In Zinc Oxide. *Phys. Rev.* **1966**, *142*, 570−574.
(46) Metwalli, E.; Pantano, C. G. Reactive Ion Etching of Glasses: Composition Dependence. *Nucl. Instrum. Methods Phys. Res., Sect. B* **2003**, *207*, 21−27.
(47) Kastenmeier, B. E. E.; Matsuo, P. J.; Beulens, J. J.; Oehrlein, G. S. Chemical Dry Etching of Silicon Nitride and Silicon Dioxide Using CF4/O2/N2 Gas Mixtures. *J. Vac. Sci. Technol., A* **1996**, *14*, 2802−2813.
(48) Zhang, H. Z.; Sun, X. C.; Wang, R. M.; Yu, D. P. Growth and Formation Mechanism of C-Oriented ZnO Nanorod Arrays Deposited on Glass. *J. Cryst. Growth* **2004**, *269*, 464−471.
(49) Zhan, Z. Y.; Liu, C.; Zheng, L. X.; Sun, G. Z.; Li, B. S.; Zhang, Q. Photoresponse of Multi-walled Carbon Nanotube-Copper Sulfide (MWNT-CuS) Hybrid Nanostructures. *Phys. Chem. Chem. Phys.* **2011**, *13*, 20471−20475.
(50) Lu, J.; Xu, C.; Dai, J.; Li, J.; Wang, Y.; Lin, Y.; Li, P. Improved UV Photoresponse of ZnO Nanorod Arrays by Resonant Coupling with Surface Plasmons of Al Nanoparticles. *Nanoscale* **2015**, *7*, 3396−3403.
(51) Tian, C.; Jiang, D.; Li, B.; Lin, J.; Zhao, Y.; Yuan, W.; Zhao, J.; Liang, Q.; Gao, S.; Hou, J.; Qin, J. Performance Enhancement of ZnO UV Photodetectors by Surface Plasmons. *ACS Appl. Mater. Interfaces* **2014**, *6* (3), 2162−2166.

DOI: 10.1021/acsami.5b05811
ACS Appl. Mater. Interfaces 2015, 7, 20264−20271

(52) Soci, C.; Zhang, A.; Bao, X. Y.; Kim, H.; Lo, Y.; Wang, D. L. Nanowire Photodetectors. *J. Nanosci. Nanotechnol.* **2010**, *10*, 1430−1449.
(53) Li, Q. H.; Gao, T.; Wang, Y. G.; Wang, T. H. Adsorption and Desorption of Oxygen Probed from ZnO Nanowire Films by Photocurrent Measurements. *Appl. Phys. Lett.* **2005**, *86*, 123117.
(54) Lin, D. D.; Wu, H.; Zhang, W.; Li, H. P.; Pan, W. Enhanced UV Photoresponse from Heterostructured Ag-ZnO Nanowires. *Appl. Phys. Lett.* **2009**, *94*, 172103.
(55) Dhara, S.; Giri, P. K. Enhanced UV Photosensitivity from Rapid Thermal Annealed Vertically Aligned ZnO Nanowires. *Nanoscale Res. Lett.* **2011**, *6*, 504.

DOI: 10.1021/acsami.5b05811
ACS Appl. Mater. Interfaces 2015, 7, 20264−20271